Video Article

The Evolution of Silica Nanoparticle-polyester Coatings on Surfaces Exposed to Sunlight

Vi Khanh Truong[1], Miljan Stefanovic[1], Shane Maclaughlin[2], Mark Tobin[3], Jitraporn Vongsvivut[3], Mohammad Al Kobaisi[1], Russell J. Crawford[4], Elena P. Ivanova[1]

[1]School of Science, Faculty of Science, Engineering and Technology, Swinburne University of Technology

[2]BlueScope Steel Research

[3]Infrared Microspectroscopy Beamline, Australian Synchrotron

[4]School of Science, College of Science, Engineering and Health, RMIT University

Correspondence to: Elena P. Ivanova at eivanova@swin.edu.au

URL: https://www.jove.com/video/54309
DOI: doi:10.3791/54309

Keywords: Engineering, Issue 116, silica nanoparticle-polyester coatings, sunlight exposure, surface topography, surface chemistry, nanoscale topography, microscale topography, nanotechnology

Date Published: 10/11/2016

Citation: Truong, V.K., Stefanovic, M., Maclaughlin, S., Tobin, M., Vongsvivut, J., Al Kobaisi, M., Crawford, R.J., Ivanova, E.P. The Evolution of Silica Nanoparticle-polyester Coatings on Surfaces Exposed to Sunlight. *J. Vis. Exp.* (116), e54309, doi:10.3791/54309 (2016).

Abstract

Corrosion of metallic surfaces is prevalent in the environment and is of great concern in many areas, including the military, transport, aviation, building and food industries, amongst others. Polyester and coatings containing both polyester and silica nanoparticles (SiO_2NPs) have been widely used to protect steel substrata from corrosion. In this study, we utilized X-ray photoelectron spectroscopy, attenuated total reflection infrared micro-spectroscopy, water contact angle measurements, optical profiling and atomic force microscopy to provide an insight into how exposure to sunlight can cause changes in the micro- and nanoscale integrity of the coatings. No significant change in surface micro-topography was detected using optical profilometry, however, statistically significant nanoscale changes to the surface were detected using atomic force microscopy. Analysis of the X-ray photoelectron spectroscopy and attenuated total reflection infrared micro-spectroscopy data revealed that degradation of the ester groups had occurred through exposure to ultraviolet light to form $COO^{\cdot}$, $-H_2C^{\cdot}$, $-O^{\cdot}$, $-CO^{\cdot}$ radicals. During the degradation process, CO and CO_2 were also produced.

Video Link

The video component of this article can be found at https://www.jove.com/video/54309/

Introduction

Environmental corrosion of metals in the environment is both prevalent and costly[1-3]. A recent study conducted by the Australasian Corrosion Association (ACA) reported that corrosion of metals resulted in a yearly cost of $982 million, which was directly associated with the degradation of assets and infrastructure through metallic corrosion within the water industry[4]. From an international perspective, the World Corrosion Organization estimated that metallic corrosion was responsible for a direct cost of $3.3 trillion, over 3% of the world's GDP[5]. The process of galvanizing as a corrosion preventative method has been widely used to increase the lifespan of steel material[6]. In humid and subtropical climates, however, water tends to condense into small pockets or grooves within the surface of the galvanized steel, leading to the acceleration of corrosion rates through pit corrosion[7,8]. Thermosetting polymer coatings based on polyesters have been developed to coat the galvanized steel substrata increasing their ability to withstand humid weathering conditions for items such as satellite dishes, garden furniture, air-conditioning units or agricultural construction equipment[9-11]. Unfortunately polymer coatings on steel surfaces have been found to be considerably adversely affected by the presence of high levels of ultraviolet (*uv*) radiation[12-14]. Coatings comprised of silica nanoparticles (SiO_2) spread over a polymer layer have been widely used with a view to increasing their corrosion-, wear-, tear- and degradation-resistance[15,16]. The tendency of the protective polymeric coatings to form pores and cracks can be reduced by incorporating nanoparticles (NPs), which contribute to the passive obstruction of corrosion initiation[17,18]. Also, the mechanical stability of the protective polymeric layer can be improved by NPs inclusion. However, these coatings act as passive physical barriers and, in comparison to the galvanization approach, cannot inhibit corrosion propagation actively.

An in-depth understanding of the effect that high-levels of ultraviolet light exposure under humid conditions upon these metal coatings is yet to be obtained. In this paper, a wide range of surface analytical techniques, including X-ray photoelectron spectroscopy (XPS), attenuated total reflection infrared micro-spectroscopy (ATR IR), contact angle goniometry, optical profiling and atomic force microscopy (AFM) will be employed to examine the changes in the surface of steel coatings prepared from polyester- and silica nanoparticle-coated polyester (silica nanoparticles/polyester) after exposure to sunlight. Furthermore, the aim of this work is to give a concise, practical overview of the overall characterization techniques to examine weathered samples.

Protocol

1. Steel Samples

1. Obtain steel samples of 1 mm thickness from a commercial supplier.
   NOTE: Samples were coated with either polyester or polyester coated with silica nanoparticles.
2. Expose samples to sunlight at Rockhampton, Queensland, Australia: collect samples after one-year and five-year intervals over a total 5-year period. Cut sample panels into round discs of 1 cm diameter using hole puncher.
3. Prior to surface characterization, rinse samples with double-distilled water, and then dry using nitrogen gas (99.99%). Keep all samples in air-tight containers to prevent any air contaminants adsorbing to the surface (**Figure 1**).

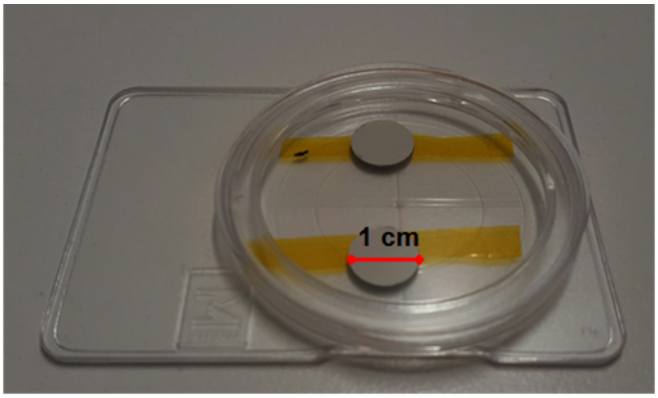

Figure 1. Preparation of metal discs with polyester-based coating. Samples were stored in containers until required. Please click here to view a larger version of this figure.

2. Chemical and Physicochemical Characterization of Surfaces

1. Analyze surface chemistry using X-ray photoelectron spectroscopy.
   1. Perform X-ray photoelectron spectrometry (XPS) using a monochromatic X-ray source (Al Kα, hv = 1486.6 eV) operating at 150 W.
      NOTE: Spot size of utilized X-ray beam is 400 µm in diameter.
   2. Load samples on the sample plate. Place the sample plate into vacuum chamber of XPS then pump the chamber. Wait for the vacuum in the chamber to reach ~1 × 10^{-9} mbar.
   3. In the photoelectron spectroscopy software, press the option of "Flood Gun" to flood the samples with low-energy electrons to counteract surface charging.
   4. Press "Insert">"Point">"Point" to insert an analysis point.
      NOTE: This will be a location at which analysis is performed. Enable the auto height function to obtain the best height for acquisition.
   5. Press "Insert">"Spectrum">"Multi Spectrum" to add scans to this point.
      NOTE: This will open a window with a periodic table; select an element by clicking on it to highlight it.
   6. After setting up the experiments, press the "Play" command to proceed the scans.
   7. Press "Peak Fit" command then press "Add Peak" and "Fit All Level" commands to resolve the chemically distinct species in the high-resolution spectra.
      NOTE: This step will acquire the Shirley algorithm to remove the background and Gaussian-Lorentzian fitting to deconvolute the spectra[19].
   8. Select all high-resolution and survey spectra. Press "Charge Shift" option to correct spectra using the hydrocarbon component of the C 1s peak (binding energy 285.0 eV) as a reference.
   9. After charge correction, press "Export" option to generate the data table of the relative atomic concentration of elements on the basis of the peak area.

2. Surface chemistry
   NOTE: Analyze surface chemistry using attenuated total reflection infrared micro-spectroscopy (ATR-IR) on the infrared (IR) spectroscopy beamline at the Australian Synchrotron as following:
   1. Load samples on the stage of microscope. Open a "Start Video Assisted Measurement" or "Start Measurement without 3D" option. Turn "VIS" mode on. Use the objective to focus on sample surface. Press "Snapshot/Overview" to take desired images.
      NOTE: 0.5 mm thick CaF_2plate can be used as the background.
   2. Change the ATR objective to the sample. Carefully move the stage to place a 45° multi-reflection germanium crystal (refractive index of 4) 1-2 mm above surfaces. Right-click on the Live Video window. Press "Start Measurement">"Change Measurement Parameters". Choose the option "Never use existing BG for all positions".
      NOTE: This will choose not to take background spectra for every measurement point.
   3. Draw a map on video screen to choose the area of interest. Press a red aperture square and choose "Aperture">"Change Aperture". Change the actual "Knife Edge Aperture" settings to X = 20 µm and Y = 20 µm.
   4. Right-click on the newly sized aperture square and go to "Aperture"> "Set all Apertures to selected Apertures". Press "Measurement" icon to start the scans. Save the data.

NOTE: The refractive index of Ge crystal is 4, so an aperture of 20 µm × 20 µm will define the spot size of 5 µm × 5 µm. This step will allow setting up FTIR mapping with an aperture of 20 by 20 µm, which corresponds to a 5 µm by 5 µm spot through the crystal across a maximum wavenumber range of 4,000-850 cm^{-1}.

5. Open master file using spectroscopy software. Choose the peak of interest on IR spectra. Right-click on the peak of interest. Choose "Integration">"Integration". It will allow creating 2D false color maps

3. Surface wettability measurements
NOTE: Perform wettability measurement using a contact angle goniometer equipped with a nanodispenser[19].
   1. Place the sample on the stage. Adjust the position of the microsyringe assembly so that the bottom of the needle appears about a fourth of a way down in the Live video window screen.
   2. Raise the sample using z-axis until distance between the sample and surface is about 5 mm. Move the syringe down until a droplet of double distilled water touches the surface. Move the syringe up to its original position.
   3. Press the "Run" command to record the water droplet impacting on the surface for a 20 sec period using a monochrome CCD Camera which is integrated with hardware.
   4. Press the "Stop" command to acquire the series of images.
   5. Press "Contact Angle" command to measure contact angles from acquired images. Repeat the contact angle measurements at three random locations for each sample.

3. Visualization of the Surface Topography

1. Optical profiling measurement.
NOTE: The instrument is operated under the white light vertical scanning interferometry mode.
   1. Place samples on the stage of the microscope.
   NOTE: Ensure there is a sufficient gap (*e.g.*, >15 mm) between objective lens and the stage.
   2. Focus on surface using the 5× objectives by controlling z-axis until the fringes appear on the screen. Press "Auto" command to optimize the intensity. Press "Measurement" command to initiate the scanning. Save the master files.
   3. Repeat the step 3.1.2 for 20× and 50× objectives.
   4. Prior to statistical roughness analyses, press "Remove Tilt" option to remove the surface waviness. Press "Contour" option to analyze the roughness parameters. Click on "3Di" option to generate three-dimensional images of optical profiling files using compatible software[20].

2. Atomic force microscopy
   1. Place samples on steel discs. Insert the steel discs into magnetic holder.
   2. Perform AFM scans in tapping mode[21]. Mechanically load phosphorus doped silicon probes with a spring constant of 0.9 N/m, tip curvature with radius of 8 nm and a resonance frequency of #20 kHz for surface imaging.
   3. Manually adjust the laser reflection on the cantilever. Choose "Auto Tune" command then press "Tune" command to tune the AFM cantilever to reach the optimum resonance frequency reported by the manufacturer.
   4. Focus on the surface. Move the tips close to sample surface. Click on Engage command to engage AFM tips on surfaces.
   5. Type "1 Hz" into scanning speed box. Choose the scanning areas. Press "Run" command to perform scan. Repeat the scanning at least for ten areas of each of five samples of each condition.
   6. Choose the leveling option to process the resulting topographical data. Save the master files.
   7. Open the compatible AFM software. Load the AFM master file. Press "Leveling" command to remove the tilting of surfaces. Press "Smoothen" command to remove the background.
   8. Press "Statistical Parameters Analysis" to generate the statistical roughness [21].

4. Statistical Analysis

1. Express the results in terms of mean value and its standard deviation. Perform statistical data processing using paired Student's two-tailed *t*-tests to evaluate the consistency of results. Set *p*-value at <0.05 indicating level of statistical significance.

Representative Results

The coated steel samples that had been subjected to exposure to the sunlight for either one or five years were collected, and water contact angle measurements were carried out to determine whether the exposure had resulted in a change in the surface hydrophobicity of the surface (**Figure 2**).

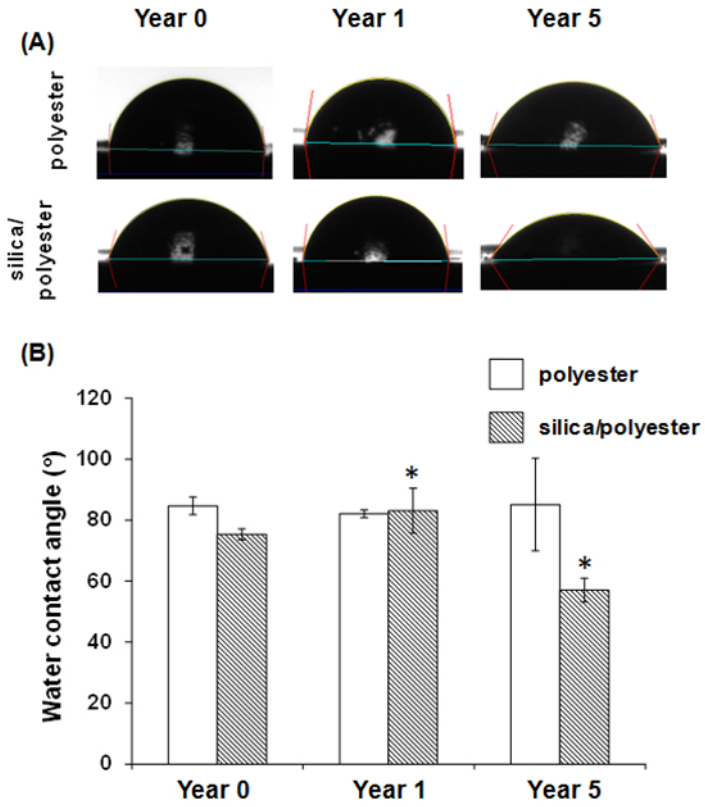

Figure 2. Wettability variation of surfaces with polyester or silica nanoparticle/polyester coatings (silica/polyester) over five years of exposure to sunlight. (**A**) Goniometric images showing the water droplet used for measuring the equilibrium contact angle of the surfaces; (**B**) Water contact angle as a function of exposure time (* indicating $p < 0.05$, compared its corresponding control (year 0)). Data represent means ± standard deviations. Please click here to view a larger version of this figure.

It was found that wettability of the polyester-coated substrata had not changed as a result of the exposure to sunlight, however the silica nanoparticle/polyester-coated samples, after one year of exposure, were found to be 1.3 times greater in hydrophobicity than the unexposed samples. Further analysis of these samples was performed using XPS and ATR-FTIR. An advantage of XPS is that this technique allows the elemental composition of a surface to be determined at a depth of approximately 10 nm below the surface. It was found that the Si content at this depth had increased from approximately 2% to 15% over the 5-year exposure period. This increase could be attributed to the adsorption of air pollutants. The XPS spectra indicated that iron (Fe) was detected on the polyester-coated substrata after one and five years of exposure (**Figure 3**) and that there had been a slight decrease in the carbon content of the polyester-coated samples after an exposure time of 5 years. No significant change was found in the silicon (Si), iron (Fe) and carbon (C) levels in the silica nanoparticle/polyester-coated substrata. XPS does not, however, allow the particular functionality of the polymer coatings to be determined. As a result, Synchrotron-sourced ATR-IR was employed to determine the changes in chemical functionality at a depth of 10 µm for the samples that had been exposed to sunlight, in particular the changes that had taken place in the number of carbonyl groups. It was found that the number of carbonyl groups decreased on both the polyester and silica nanoparticle/polyester-coated samples after five years of exposure.

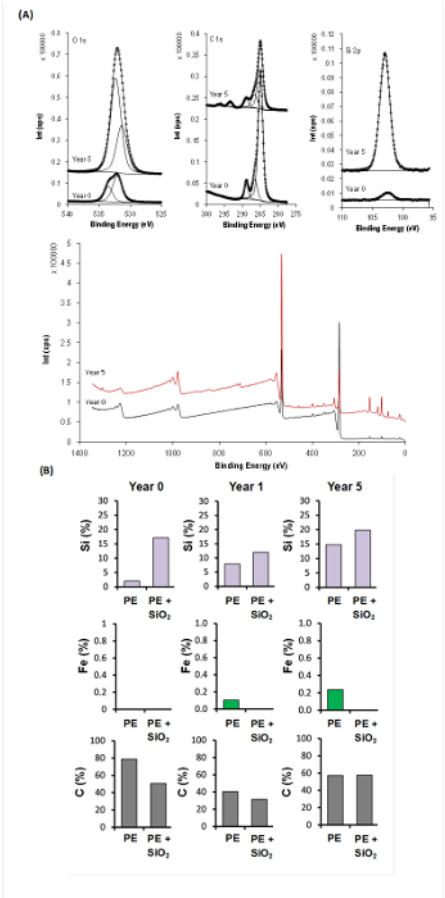

Figure 3. Elemental composition variation of polyester (PE) and silica nanoparticle/polyester coatings (PE + SiO_2) over five years exposing to sunlight as determined using XPS. (**A**) Representative XPS wide spectra and high resolution spectra of O 1s, C 1s and Si 2p of polyester coatings before and after exposure. (**B**) The concentration of three elements (Si, Fe and C) (atomic fraction) was measured as a function of time of exposure to determine changes in the composition of the surface coating under high levels of sunlight exposure under humid conditions. Please click here to view a larger version of this figure.

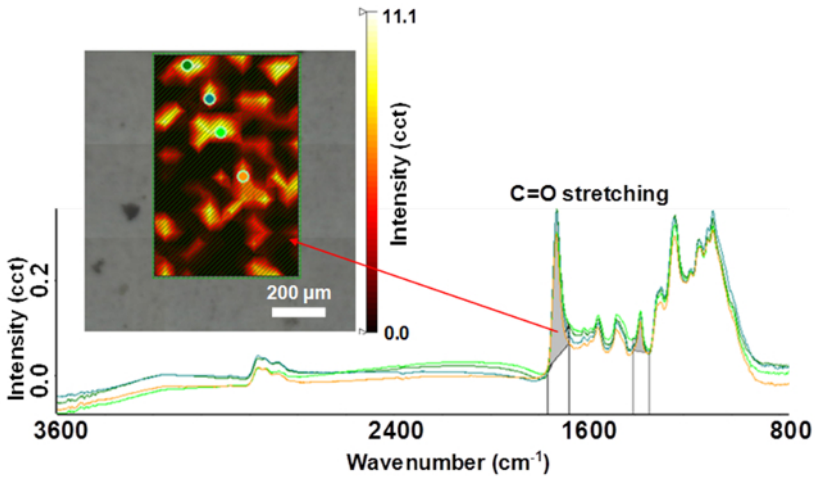

Figure 4. Representative ATR-FTIR spectra used for the measurement of changes in the carbonyl groups on the steel surface coatings after three years of environmental exposure. Changes in the distribution of carbonyl groups resulted from the ultraviolet light-induced breakdown of ester groups. Please click here to view a larger version of this figure.

Optical profiling and atomic force microscopy were further employed to investigate the surface topography of the substrata at the micro- and nano-scale. The microscale topographic evolution of the polyester and silica nanoparticle/polyester-coated samples is presented in **Figure 5**. It can be seen that the surfaces of both coatings became rougher than the original substrata, after one year of exposure, however this increase was found not to be statistically significant ($p > 0.05$).

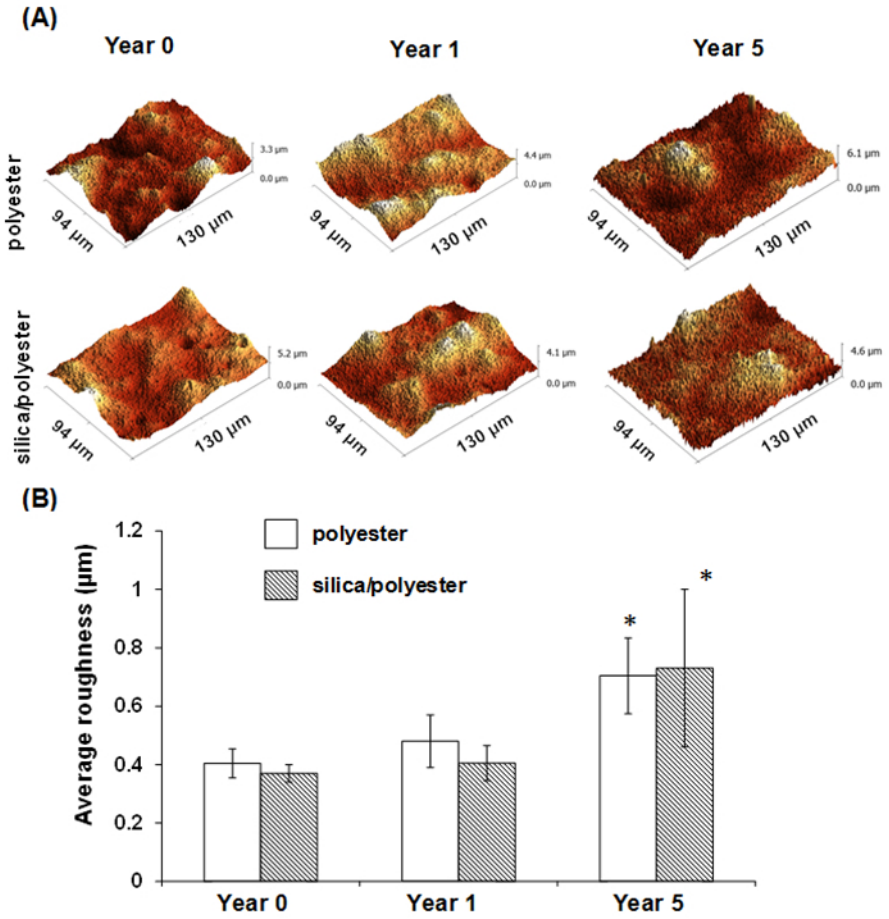

Figure 5. Micro-scale topographic changes in the polyester and silica nanoparticle/polyester coatings on steel over a five-year exposure period. (**A**) Representative optical profiling images of steel coatings before and after exposure. (**B**) Graph showing an increase in the average roughness of both coatings as a function of time of environmental exposure (* indicating $p < 0.05$, compared with its corresponding control (year 0)). Data represent means ± standard deviations. Please click here to view a larger version of this figure.

Further analysis of the substrata highlighted that the nanoscale surface topography was significantly altered as a result of the ultraviolet light exposure (**Figures 6, 7** and **8**). The original silica nanoparticle/polyester coatings were smooth on a nanometer scale, however, after exposure, these both coatings were found to have formed globular structures. After five years of exposure, the surfaces were found to exhibit a significantly higher average roughness than the original substrata, ranging from 40 - 47 nm ($p < 0.05$).

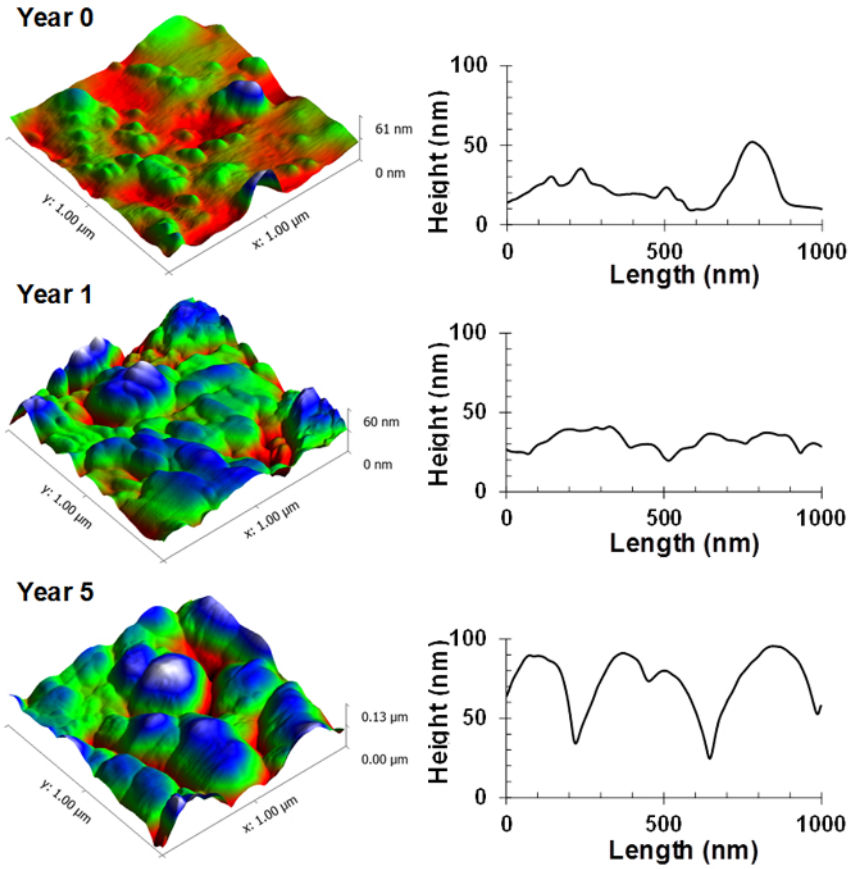

Figure 6. Nanoscale topographic changes for polyester coatings on steel over a five-year exposure period. Representative atomic force micrographs and their corresponding surface profile, highlighting the topographic changes of the polymer coating. Please click here to view a larger version of this figure.

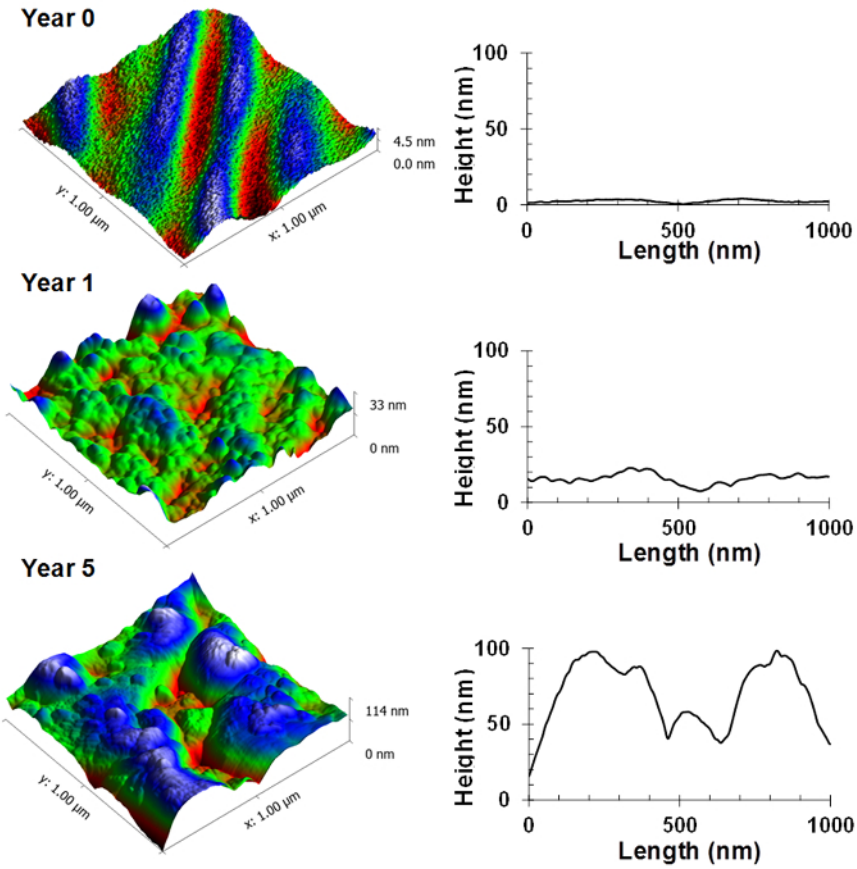

Figure 7. Nanoscale topographic changes for silica nanoparticle/polyester coatings over a five-year exposure period. Representative atomic force micrographs and their corresponding surface profile, highlighting the topographic changes of the polymer coating, despite the presence of the silica nanoparticle protection layer. Please click here to view a larger version of this figure.

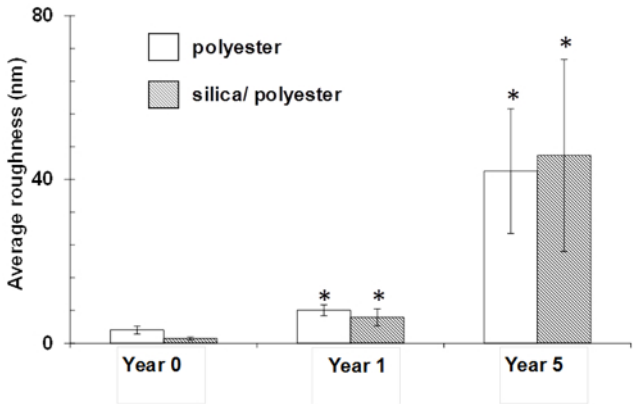

Figure 8. Average nanoscale surface roughness of polyester and silica nanoparticle/polyester coatings on steel as a function of exposure time. The average roughness of the surface coatings increases significantly with time of exposure (* indicating $p < 0.05$, compared with its corresponding control (year 0)). Data represent means ± standard deviations. Please click here to view a larger version of this figure.

Discussion

Polyester coatings have been widely used to protect steel substrata from the corrosion that would occur on an uncoated surface due to the accumulation of moisture and pollutants. The application of polyester coatings can protect the steel from corrosion; however the longer-term effectiveness of these coatings is compromised if they are exposed to high levels of ultraviolet light under humid conditions, as occurs in tropical climates. Silica nanoparticles can be applied to the surface of the polyester to improve the robustness of these coatings within these environments, however the effect of environmental factors on these silica-containing coating materials was, until now, unknown, particularly in regard to changes in their micro- and nanoscale surface topography.

In many cases, the wettability of a substratum surface can provide an indication as to whether any surface degradation has taken place. Contact angle measurements, however, do not provide any detail regarding the physical and chemical structural changes that may have taken place on a surface (**Figure 2**). XPS and ATR-FTIR are techniques that allow changes in the carbon content and carbonyl (C=O) functionality distribution to be determined.

The results obtained in this study suggest that sunlight exposure causes the degradation of polyester coatings. A proposed mechanism for this degradation is given in **Figure 9**[22,23]. Ester groups can be radically degraded through exposure to ultraviolet light to form radical -COO·, -H_2C·, -O·, -CO·. During the degradation process, CO and CO_2 are produced.

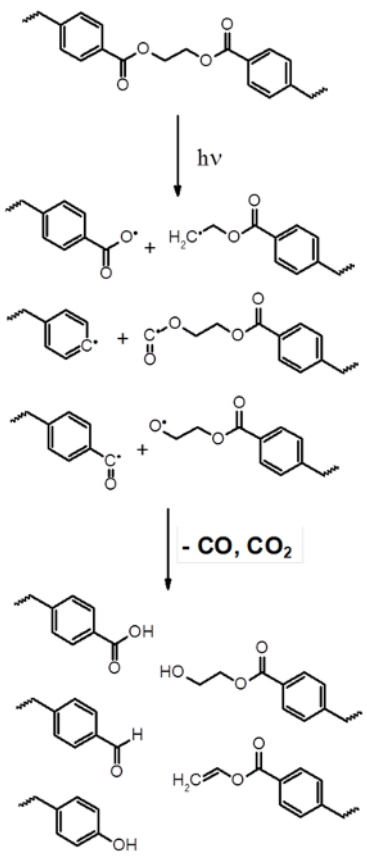

Figure 9. Proposed ultraviolet light-catalyzed degradation of polyester. Under exposure to sunlight, the ester groups present on the polyester formed radical species to form stable alcohol, aldehyde, carboxylic acid groups with the elimination of carbon monoxide and carbon dioxide. Please click here to view a larger version of this figure.

In addition to the chemical degradation of the coatings, changes in the surface topography of the coatings were observed, but only on the nanoscale. In previous studies, ultraviolet light irradiation was also reported to have significantly modified the surface nanoscale topography of polymer surfaces[24-26]. Here, it was found that the surface topology had been changed through the formation of globular nanoscale structures (**Figures 6** and **7**).

XPS can provide an insight into changes in surface chemistry at level of part per million. Due to the high sensitivity of the technique, sample contamination can be readily detected and this may lead to biased results. The most important step in preparation of the samples for XPS analysis is to ensure that the samples do not outgas or contain any particles that may damage the vacuum system of the instrument. To prevent this from occurring, samples should be cleaned using nitrogen gas and degassed before any measurement. This technique only provides the overall chemistry of a surface over a few hundreds of micrometers, and only reveals the surface chemistry to a depth of ~10 nm. The resulting high resolution spectra allow the different chemical species existing on surfaces to be determined. XPS is an important tool for the investigation of chemical modifications of the surface that may occur. An alternative technique to XPS is energy-dispersive X-ray spectroscopy (EDX)[27].

ATR-IR microscopy requires that a good contact exists between the ATR crystal and the surface being analyzed because of the small extension of the evanescent wave that occurs beyond the crystal. ATR-IR microscopy spatially resolves the molecular and structural composition of surfaces. Contamination of the ATR crystal can also cause a low signal or biased results to be obtained. Prior to any experiment, it is important to clean the crystal with pure isopropanol to ensure that any cross-contamination does not occur. Also, the refractive index of the ATR crystal must be significantly higher than that of the sample. Infrared (IR) spectroscopy using the ATR method is able to be applied to the chemical or biological systems that can be analyzed using the transmission method. ATR-IR has been widely used to monitor the development of eukaryotic cells. Raman micro-spectroscopy is an alternative method by which the chemical heterogeneity of surface can be determined[28].

Water contact angle goniometry is a technique, based upon the Young equation, determined the hydrophobicity of a solid surface. When using this technique, samples should be appropriately stored, such that adsorption of any contaminant can be avoided. A limitation of this technique is that it is restricted to flat surfaces. If this is not the case, the curvature at liquid/solid/air interface will be distorted and undefined. This technique is widely used to indicate any chemical change that may have occurred on a surface, and to determine the presence of hydrophobic and hydrophilic functionalities. The Wilhelmy plate method is an alternative (but less easily performed) technique for estimating the degree of surface wettability[29].

Optical surface profiling provides a nondestructive and noncontact metrology. The most critical step of this technique requires users to commence measurements at the lowest magnification in order to define the focal plane and prevent contact between the objective lens and the sample surface. Optical profiling only allows the visualization of the surface topography on the micro-scale. Atomic force microscopy has the ability to examine the topography of a surface from the nano- to molecular-scale. Operation of the AFM requires specific skills and a greater time for analysis compared to optical profiling. The current study provides an excellent example where AFM was able to detect changes in surface topography that were not evident using optical profiling. Alternative techniques to optical profiling and AFM are stylus profiling and scanning electron microscopy, which can also provide the quantification of surface architecture[27,30].

A set of these surface characterization techniques can be used to investigate chemical and topographic characteristics of polymer and metallic surfaces. Optical profiling and atomic force microscopy can be used to examine changes in the surface micro- and nano-scale topography. Surface chemical characterization techniques including IR-microscopy and X-ray photoelectron spectroscopy can be utilized to laterally examine the surface chemistry homogeneity.

Disclosures

The authors have nothing to disclose.

Acknowledgements

Funding from the Australian Research Council Industrial Transformation Research Hubs Scheme (Project Number IH130100017) is gratefully acknowledged. Authors gratefully acknowledge the RMIT Microscopy and Microanalysis Facility (RMMF) for providing access to the characterisation instruments. This research was also undertaken on the Infrared Microscopectroscopy beamline at the Australian Synchrotron, Victoria, Australia.

References

1. Fathima Sabirneeza, A. A., Geethanjali, R., & Subhashini, S. Polymeric corrosion inhibitors for iron and its alloys: A review. *Chem. Eng. Commun.* **202**(2), 232-244 (2015).
2. Gupta, R. K., & Birbilis, N. The influence of nanocrystalline structure and processing route on corrosion of stainless steel: A review. *Corros. Sci.* **92** 1-15 (2015).
3. Lee, H. S., Ismail, M. A., & Choe, H. B. Arc thermal metal spray for the protection of steel structures: An overview. *Corros. Rev.* **33**(1-2), 31-61 (2015).
4. Moore, G. Corrosion challenges - urban water industry *The Australasian Corrosion Association Inc.*, (2010).
5. Hays, G. F. *World Corrosion Organization.* (2013).
6. Koch, G. H., Brongers, M. P. H., Thompson, N. G., Virmani, P. Y., & Payer, J. H. Corrosion cost and preventive strategies in the United States. *CC Technologies Laboratories, Incorporated; NACE International; Federal Highway Administration, NACE International.* (2002).
7. Pojtanabuntoeng, T., Singer, M., & Nesic, S. in *Corrosion '2011*. Houston, TX, (2011).
8. Jašniok, T., & Jašniok, M. in *7'th Scientific-Technical Conference on Material Problems in Civil Engineering, MATBUD '2015'*. eds T. Tracz & I. Hager) 316-323 (Elsevier Ltd) (2015).
9. Cambier, S. M., Posner, R., & Frankel, G. S. Coating and interface degradation of coated steel, Part 1: Field exposure. *Electrochim. Acta.* **133** 30-39 (2014).
10. Barletta, M., Gisario, A., Puopolo, M., & Vesco, S. Scratch, wear and corrosion resistant organic inorganic hybrid materials for metals protection and barrier. *Mater. Des.* **69** 130-140 (2015).
11. Fu, J. *et al.* Experimental and theoretical study on the inhibition performances of quinoxaline and its derivatives for the corrosion of mild steel in hydrochloric acid. *Ind. Eng. Chem. Res.* **51**(18), 6377-6386 (2012).
12. Hattori, M., Nishikata, A., & Tsuru, T. EIS study on degradation of polymer-coated steel under ultraviolet radiation. *Corros. Sci.* **52**(6), 2080-2087 (2010).
13. Yang, X. F. *et al.* Weathering degradation of a polyurethane coating. *Polym. Degrad. Stab.* **74**(2), 341-351 (2001).
14. Armstrong, R. D., Jenkins, A. T. A., & Johnson, B. W. An investigation into the uv breakdown of thermoset polyester coatings using impedance spectroscopy. *Corros. Sci.* **37**(10), 1615-1625 (1995).
15. Zhou, W., Liu, M., Chen, N., & Sun, X. Corrosion properties of sol-gel silica coatings on phosphated carbon steel in sodium chloride solution. *J. Sol. Gel. Sci. Technol.* **76**(2), 358-371 (2015).
16. Hollamby, M. J. *et al.* Hybrid polyester coating incorporating functionalized mesoporous carriers for the holistic protection of steel surfaces. *Adv. Mater.* **23**(11), 1361-1365 (2011).
17. Borisova, D., Möhwald, H., & Shchukin, D. G. Mesoporous silica nanoparticles for active corrosion protection. *ACS Nano.* **5**(3), 1939-1946 (2011).
18. Wang, M., Liu, M., & Fu, J. An intelligent anticorrosion coating based on pH-responsive smart nanocontainers fabricated via a facile method for protection of carbon steel. *J. Mater. Chem. A.* **3**(12), 6423-6431 (2015).
19. Truong, V. K. *et al.* The influence of nano-scale surface roughness on bacterial adhesion to ultrafine-grained titanium. *Biomaterials.* **31**(13), 3674-3683 (2010).

20. Nečas, D., & Klapetek, P. Gwyddion: An open-source software for SPM data analysis. *Cent. Eur. J. Phys.* **10**(1), 181-188 (2012).
21. Crawford, R. J., Webb, H. K., Truong, V. K., Hasan, J., & Ivanova, E. P. Surface topographical factors influencing bacterial attachment. *Adv. Colloid Interface Sci.* **179-182** 142-149 (2012).
22. Allen, N. S., Edge, M., Mohammadian, M., & Jones, K. Physicochemical aspects of the environmental degradation of poly(ethylene terephthalate). *Polym. Degrad. Stab.* **43**(2), 229-237 (1994).
23. Newman, C. R., & Forciniti, D. Modeling the ultraviolet photodegradation of rigid polyurethane foams. *Ind. Eng. Chem. Res.* **40**(15), 3346-3352 (2001).
24. Ivanova, E. P. *et al. Vibrio fischeri* and *Escherichia coli* adhesion tendencies towards photolithographically modified nanosmooth poly (*tert*-butyl methacrylate) polymer surfaces. *Nanotechnol. Sci. Appl.* **1** 33-44 (2008).
25. Biggs, S., Lukey, C. A., Spinks, G. M., & Yau, S. T. An atomic force microscopy study of weathering of polyester/melamine paint surfaces. *Prog. Org. Coat.* **42**(1-2), 49-58 (2001).
26. Signor, A. W., VanLandingham, M. R., & Chin, J. W. Effects of ultraviolet radiation exposure on vinyl ester resins: Characterization of chemical, physical and mechanical damage. *Polym. Degrad. Stab.* **79**(2), 359-368 (2003).
27. Wang, H. *et al.* Corrosion-resistance, robust and wear-durable highly amphiphobic polymer based composite coating via a simple spraying approach. *Prog. Org. Coat.* **82** 74-80 (2015).
28. Liszka, B. M., Lenferink, A. T. M., Witkamp, G. J., & Otto, C. Raman micro-spectroscopy for quantitative thickness measurement of nanometer thin polymer films. *J. Raman Spectrosc.* **46**(12), 1230-1234 (2015).
29. Alghunaim, A., Kirdponpattara, S., & Newby, B. M. Z. Techniques for determining contact angle and wettability of powders. *Powder Technol.* **287** 201-215 (2016).
30. Treviño, M. *et al.* Erosive wear of plasma electrolytic oxidation layers on aluminium alloy 6061. *Wear.* **301**(1-2), 434-441 (2013).

